(Preprint) AAS 25-185

EXPANDED BACKSUBSTITUTION DYNAMICS MODELING FOR BRANCHED FORCE AND TORQUE BASED SPACECRAFT COMPONENTS

Andrew Morell* **and Hanspeter Schaub†**

Classic spacecraft architectures include a collection of components mounted in parallel to a common central hub. As new missions propose increasingly complex architectures, performance gains are sought through mounting actuators to moving platforms instead of directly to this central hub to achieve controllable degrees of freedom or larger moment arms. This added vehicle complexity must be matched with more realistic modeling and simulation to capture the added dynamical complexity. The backsubstitution method (BSM) is a dynamics formulation that enables modular spacecraft equations of motion with computational efficiency in simulation. The BSM historically assumes a classic spacecraft architecture, but is now expanded to support the dynamical modeling of components branched off of other components, preserving its modularity while enabling these more complex spacecraft architectures. Mathematical alterations are made to the BSM to allow components which exclusively generate forces and torques without a time varying geometry to be attached to such a time varying geometry. The Basilisk Simulation Framework is chosen for implementation as an existing simulator which leverages the BSM and is designed for spacecraft. The dynamical differences between this branched architecture and a strictly hub centric implementation of the same parameters are highlighted through comparison of their resulting motion with a thruster attached. The model is successively stress tested with more complex scenarios that highlight the added capability. The branched design results in more intuitive motion of the motion platform flexing ahead of its central hub, whereas the traditional design results in the motion platform lagging behind its central hub.

INTRODUCTION

The complexity of spacecraft designs are continuously increasing as underlying technology advancements enable more ambitious vehicle architectures and objectives. Lightweight robotic arms on spacecraft add degrees-of-freedom (DOF) useful for dexterous tasks such as on-orbit servicing and thruster pointing, but introduce lower frequency resonant modes to be excited. Deployable solar arrays increase surface area for additional power, but add sensitivity to torques from drag, solar radiation pressure, and gravity gradient. As mission concepts advance in these ways, the modeling and simulation that validate and verify their flight dynamics also require improvement to capture the dynamical effects introduced.

The Backsubstitution Method (BSM) is one such improvement that enabled modularity for complex spacecraft modeling, including flexible and multibody dynamics with enhanced computational

*Graduate Research Assistant, Ann and H.J. Smead Department of Aerospace Engineering Science, University of Colorado, Boulder, 431 UCB, Colorado Center for Astrodynamics Research, Boulder, CO, 80309.

†Distinguished Professor and Department Chair, Schaden Leadership Chair, Ann and H.J. Smead Department of Aerospace Engineering Sciences, University of Colorado, Boulder, 431 UCB, Colorado Center for Astrodynamics Research, Boulder, CO, 80309. AAS Fellow, AIAA Fellow

efficiency.[1,2] These original gains by the BSM were accompanied by the assumption of a classic BSM spacecraft architecture. Thinking of spacecraft architectures as a collection of components mounted around a central hub structure, a classic architecture attaches all components directly to the central hub in parallel. However, modern space missions are pursuing structural complexity such that this assumption can no longer be observed. Spacecraft components historically mounted statically to a central hub are in mission concepts attached to mobile structures, and components with legacy on mobile platforms are seen on thinner or higher-DOF structures. Some examples are Astroscale's Life Extension In-orbit (LEXI) spacecraft, Northrop Grumman's Mission Robotic Vehicle (MRV) and Mission Extension Pod (MEP), and NASA's Mars Reconnaissance Orbiter (MRO) shown in Figure 1.[3–5] The LEXI spacecraft hosts four 2-DOF arms with thrusters attached at the ends, and four other 2-DOF robotic arms for docking. The MEP is itself held by the MRV using two multi-DOF robotic arms, and then has its own singular multi-DOF robotic arm with a thruster mounted at the end. The MRO has two solar panels whose large surface area was used for aerobraking around Mars, subject to deflection from drag forces similar to the Mars Global Surveyor (MGS).[6] Other proposed missions sporting similar use of robotic arms for docking include the European Space Agency's Clearspace-1, NASA's OSAM-1, and Starfish Space's Otter.[7–9] Each of these arms, when fully extended, has the potential to experience significant deflection when thrust, grappling, or environmental forces occur at their ends.

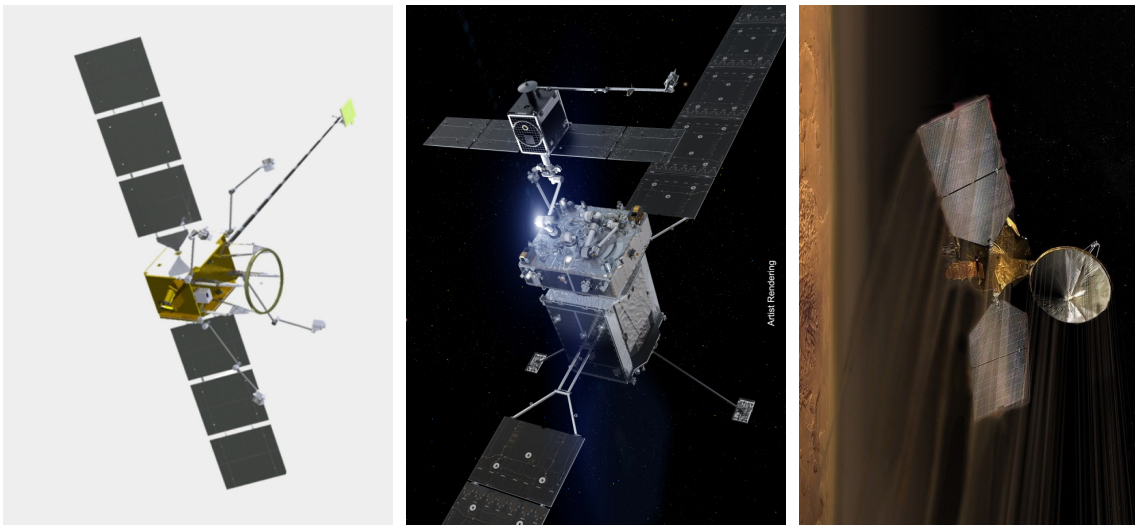

(a) Astroscale's LEXI [10].

(b) Northrop Grumman's MRV and MEP [11].

(c) NASA's MRO [5].

Figure 1. Model renders of spacecraft component branching architectures.

The BSM achieves its modularity and computational efficiency through the use of particular analytical forms of the equations of motion (EOMs) of a spacecraft and its attached components. Although the BSM is capable of modeling these cases of branched dynamical effects shown in Figure 1, it requires a custom analytical derivation for each unique permutation of attached components, therefore losing its convenience of modularity. This work presents a modern adaptation of the BSM allowing branched dynamical components to be attached interchangeably and therefore extending modularity to these scenarios.

These cases in which a component's attachment to its central hub is not considered rigid are

referred to as time-varying geometries and in the context of space missions can be grouped into some intuitive categories of multibody dynamics modeling considerations. This work considers categories corresponding to the modeled forces and torques driving the time-varying geometries, as well as categories of dynamical topology grouped according to spacecraft architecture.

The paper is structured as follows. A background section identifies how the BSM is expanded relative to prior work. The problem formulation outlines the exact challenges and their successive solutions followed by a mathematical overview of the modifications to the BSM. Next, in the numerical results section, results showing the platform deflection and corresponding hub motion are shown for different thruster and arm configurations. Discussions of the advantages of using each modeling category over another are provided, highlighting trade-offs between the complexity of the model setup, computation time, and realism.

BACKGROUND

Three types of joint motion are identified that provide context as to what forces and torques are considered: actuated, hub-excited flexing, and component-excited flexing. Previous developments in the first two categories are highlighted, and the third category is proposed as a previously unexplored problem within the BSM. Three categories of dynamical topology are also identified: linear branches, divergent branches, and closed-loop chains. The goal of these breakdowns is to highlight improvements in the fidelity of modeling and simulation of how the spacecraft and its associated structures move.

Joint Motion Classification

In the case of actuated joints, components are mounted on an intermediate platform on the central hub in order to provide controllable DOFs to the component. Forces and torques are directly applied at a joint to change the configuration in which a component is in, and reactionary forces and torques must be applied to the parent body. For example, solar arrays and communication antennas can be gimbaled in 1-DOF or 2-DOF to enable more optimal vehicle pointing configurations. Thrusters are gimbaled on larger spacecraft to align thrust forces with the vehicle's center of mass, minimizing undesired torque generation. Robotic arms can be thought of as a series of intermediate platforms that can host grappling end effectors on vehicles performing docking operations. The dynamics of generalized multibody systems in the context of free-flying spacecraft is thoroughly studied in the literature.[12–14] These structures are commonly assumed to be rigid bodies attached to the central hub with no flexing motion outside of what is commanded at the joint. When these rigid on rigid and purely controlled assumptions are made, their motion is considered to be prescribed, meaning that a modeled intermediate platform moves along a planned path without considering external forces.[15] The BSM has been expanded to model purely prescribed motion in several prior works, fundamentally in Reference (16), and later implemented for N-DOF deployable translational or rotational bodies.[16–18]

While actuated joints assume rigid bodies connected by a prescribed joint, passive flexibility of joints is concerned with uncontrolled motion due to the natural stiffness and damping in the structure. Although some of this structural flexing occurs in the bodies on either side of a joint, when modeled, all of the flexing is approximated as deflection at the joint itself between a rigid platform and its rigid parent body. In the case of hub-excited flexing, the forces and torques of interest at the joint result from an excitation by the movement of the central hub and the inertia of a component platform lagging behind. For example, non-actuated solar panels that are large with respect to their

central hub may still move during a slew maneuver with respect to their central hub because of the underlying structure flexing. Other large yet thin passive components susceptible to structural flexing include booms for gravity gradient stability and antennas, which motivate consideration when modeling dynamics. Previous work has utilized some of the same methods used for modeling traditional multibody dynamics, such as Kane's method,[14] but with the joint loosened to a flexible assumption.[19,20] The BSM supported this hub excited flexing from its inception and has specifically implemented hub-excited flexing with solar panels, fuel slosh, revolute robotic arms, and translating bodies.[19,21–24]

The case of component-excited flexing is applied to the same types of flexibly susceptible structures but instead focuses on forces and torques at the joint resulting from the movement of the attached body and the inertia of the parent body lagging behind. In this case a force is applied directly to the attached body, for example a thruster mounted on a robotic arm as shown in Figure 1(a), which accelerates with the central hub reacting. Compared to a classic spacecraft configuration with thrusters mounted directly to the central hub, this thruster arm will flex in the opposite direction than if the acceleration was applied directly to the central hub. Additionally, the magnitude of deflection will be larger assuming that its inertia is smaller than that of the central hub structure. This component excited flexing is solved in alternative dynamical approaches, including finite element analysis (FEA) and spatial operator algebra (SOA). This component excited flexing is also achievable using the BSM in its classical form but requires the legwork of analytically deriving custom equations of motion for every permutation of components as detailed in the following section: Mathematical Overview of BSM. The novelty presented in this work is an enhanced BSM that preserves its existing modularity such that the dynamical models of components can be interchangeably attached, applying forces and torques from a variety of components on a variety of bodies stemming from the central hub.

It is important to note that these three categories of modeling forces and torques for actuated and passively flexing components are not mutually exclusive. The flexing of a structure about some nominally actuated configuration can be considered, achieving a combination of the modeling considerations. For example, a solar panel may be actuated to be pointing at different angles with respect to its central hub when that central hub performs orbital maneuvers, and therefore the resulting flexing would occur in different directions with respect to the hub-panel connection. Alternatively, if the central hub is inactive, not producing any external forces or torques on the environment, and instead quickly slews its solar panels to a different configuration, those panels could flex as their motion lags behind what is being commanded at the connection joint. This has historically been studied in the context of deployment maneuvers.[25,26]

Joint Topology Classification

With an understanding of where branched forces and torques fit relative to prior force and torque based components in the BSM, it is also useful to identify different ways in which this branching can be applied. These categories of branching in the BSM are organized by dynamical topology as linear branches, divergent branches, and closed-loop chains. With the goal of improving realism in the modeling and simulation of how a spacecraft and its associated structures move, this breakdown seeks a more intuitive dichotomy of what can and cannot be modeled using this expanded form of the BSM.

When analyzing dynamical topology in BSM, it is useful to distinguish between different types of components. The term effector is used to refer to any dynamical consideration applied to a

spacecraft's central hub. When using the BSM, these effectors are broken out into two subcategories: dynamic effectors and state effectors. State effectors represent components with associated states that are coupled with the central hub and must be integrated, such as the angles and angle rates of a revolute gimbal solar panel, or robotic arm. Dynamic effectors represent components that influence the spacecraft through generating forces and torques, but do not have states to be integrated. For example, actuators such as thrusters or docking mechanisms, and dynamical effects including solar radiation pressure (SRP) or drag. In the dynamical topology shown in Figure 2, state effectors are shown in gold, and dynamic effectors are shown in blue.

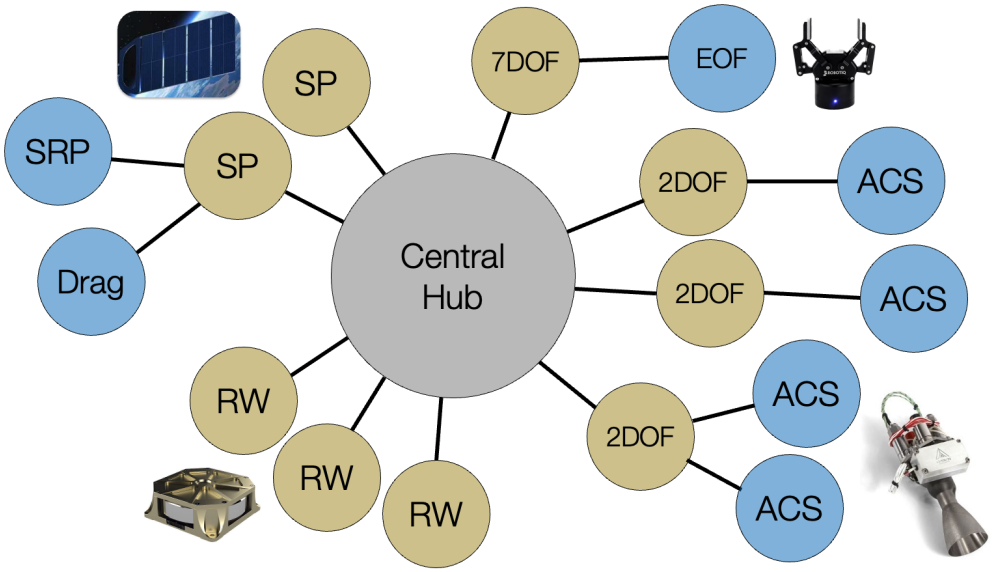

Figure 2. Dynamical branching topology with reaction wheels (RW), solar panels (SP), solar radiation pressure (SRP), end effector (EOF), and attitude control thrusters (ACS).

In this new dichotomy, linear branching denotes a series of sequential effectors extending from a central hub that can be thought of as linearly stacked. Therefore, a linear branching topology, for example, could be a segmented translating robotic arm with a grappling end effector for docking such as the one shown in Figure 2. Divergent branching refers to a tree of effectors extending from a singular connection to the central hub but with multiple ending leaf nodes. For example, a 3-DOF revolute robotic arm with drag applied to each of the three segments and a thruster attached to the third segment. A closed-loop chain is any tree of effectors, linear or divergent, that has more than one child node at the central hub. For example, a torus-shaped space station composed of five segments.

Reference (27) surveys existing BSM work to show that linear branching is historically the only permissible form of branching in the classic BSM. Reference (28) explores linear branching scenarios, but not divergent and closed-loop varieties. Reference (28) also demonstrates the initial proof of concept by implementing the 1-DOF linear branching. This work fully explores both linear branching and divergent branching in a generalized analytical formulation and implemented in simulation.

PROBLEM FORMULATION

The application of forces and torques along flexible structures proposes challenges in dynamical modeling, as some external forces and torques generated on a flexing structure must exert those external influences according to inertial states which are propagated at the central hub level. For example, forces and torques due to solar radiation pressure (SRP) on a large solar array or sail are dependent on the array's orientation with respect to the Sun, so those computations become dependent on both the central hub's orientation and the panel's deflection at its joint to the hub. The challenge ultimately lies in ensuring that this dynamical linking preserves the modularity of the BSM to provide a generalized solution.

In order to expand the BSM to enable this component excited flexing, the modular architecture is adapted to allow components to be attached to moving platforms on a spacecraft rather than exclusively on a central hub. This branching off of components on other components is only applicable to selective configurations. The expansion of the BSM in this work enables dynamic effectors to be attached to a state effector, but does not enable a state effector to branch off of any other type of effector.

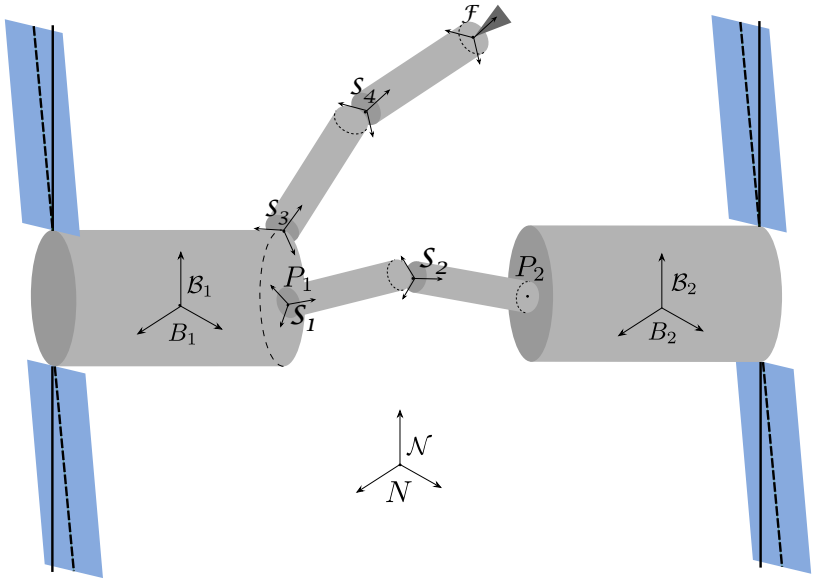

Figure 3. Component branching example configuration.

An example configuration is shown in Figure 3. There are two 2-DOF robotic arms: one connecting the two rigid hubs B_1 and B_2, and another mounting a thruster $\mathcal{F}$ to the hub B_1. The classic BSM requires that analytical equations of motion (EOMs) be derived for a thruster at the end of a 2-DOF gimbaled arm and a constraint effector at the end of a 2-DOF arm in order to simulate the dynamics of this scenario. With the modern architecture, pre-existing analytical models of a revolute robotic arm, thruster, and constraint effector can be stacked without any additional analytical setup to model this scenario.

When arranging the dynamics of these different types of effectors into the BSM, Basilisk first sums the forces and torques of all dynamic effectors assuming them to act on the central hub. Then Basilisk compiles the contributions to the hub's translational and rotational states by state effectors. For component excited flexing, dynamic effectors attached to a state effector instead have

their generated forces and torques summated by their parent state effector, which then passes the accelerations to the central hub within its own EOM contributions.

MATHEMATICAL OVERVIEW OF BSM

To understand applying component excited flexing in the context of the BSM, it is beneficial to first lay out the relevant terms used in this method from Reference (29). Note that bold variables $\boldsymbol{x}$ implies a vector quantity, $\dot{\boldsymbol{x}}$ denotes an inertial time derivative of $\boldsymbol{x}$, whereas $\boldsymbol{x}'$ denotes a fixed frame relative time derivative, and $[\tilde{\boldsymbol{x}}]\boldsymbol{y}$ is the matrix cross product notation. Eq. (1) shows the compact form of the coupled translational and rotational EOMs of the spacecraft hub using subscripts consistent with reference frames defined in Figure 3.

$$\begin{bmatrix}[A][B]\\[C][D]\end{bmatrix}\begin{bmatrix}\ddot{\boldsymbol{r}}_{B/N}\\\dot{\boldsymbol{\omega}}_{B/N}\end{bmatrix}=\begin{bmatrix}\boldsymbol{v}_{\text{Trans}}\\\boldsymbol{v}_{\text{Rot}}\end{bmatrix} \tag{1}$$

Here $\ddot{\boldsymbol{r}}_{B/N}$ is the inertial translational acceleration between body fixed point B on the spacecraft hub and inertially fixed point N, and $\dot{\boldsymbol{\omega}}_{B/N}$ is the inertial angular acceleration between body fixed frame $\mathcal{B}$ and inertially fixed frame $\mathcal{N}$. These translational and rotational EOMs of the spacecraft's central hub are decoupled from the states of other component effectors which are grouped into the matrices $[A]$, $[B]$, $[C]$, and $[D]$ and vectors $\boldsymbol{v}_{\text{Trans}}$ and $\boldsymbol{v}_{\text{Rot}}$ shown in Eqs. (2)-(3).

$$[A]=m_{\text{sc}}\,[I_{3\times3}]+\sum_{i=1}^{N_{\text{eff}}}\boldsymbol{v}_{\text{Trans,LHS}_i}\boldsymbol{a}_{\alpha_i}^T \tag{2a}$$

$$[B]=-m_{\text{sc}}\,[\tilde{\boldsymbol{c}}]+\sum_{i=1}^{N_{\text{eff}}}\boldsymbol{v}_{\text{Trans,LHS}_i}\boldsymbol{b}_{\alpha_i}^T \tag{2b}$$

$$[C]=m_{\text{sc}}\,[\tilde{\boldsymbol{c}}]+\sum_{i=1}^{N_{\text{eff}}}\boldsymbol{v}_{\text{Rot,LHS}_i}\boldsymbol{a}_{\alpha_i}^T \tag{2c}$$

$$[D]=[I_{\text{sc},B}]+\sum_{i=1}^{N_{\text{eff}}}\boldsymbol{v}_{\text{Rot,LHS}_i}\boldsymbol{b}_{\alpha_i}^T \tag{2d}$$

$$\boldsymbol{v}_{\text{Trans}}=\boldsymbol{F}_{\text{ext}}-2m_{\text{sc}}[\tilde{\boldsymbol{\omega}}_{\mathcal{B}/\mathcal{N}}]\boldsymbol{c}'-m_{\text{sc}}[\tilde{\boldsymbol{\omega}}_{\mathcal{B}/\mathcal{N}}][\tilde{\boldsymbol{\omega}}_{\mathcal{B}/\mathcal{N}}]\boldsymbol{c}+\sum_{i=1}^{N_{\text{eff}}}[\boldsymbol{v}_{\text{Trans,RHS}_i}-\boldsymbol{v}_{\text{Trans,LHS}_i}c_{\alpha_i}] \tag{3a}$$

$$\boldsymbol{v}_{\text{Rot}}=\boldsymbol{L}_B-[\tilde{\boldsymbol{\omega}}_{\mathcal{B}/\mathcal{N}}]\,[I_{\text{sc},B}]\,\boldsymbol{\omega}_{\mathcal{B}/\mathcal{N}}-[I'_{\text{sc},B}]\boldsymbol{\omega}_{\mathcal{B}/\mathcal{N}}+\sum_{i=1}^{N_{\text{eff}}}[\boldsymbol{v}_{\text{Rot,RHS}_i}-\boldsymbol{v}_{\text{Rot,LHS}_i}c_{\alpha_i}] \tag{3b}$$

Here m_{sc} is the total mass of the spacecraft, $\boldsymbol{c}$ is the vector from body fixed point B to the center of mass (COM) of the spacecraft C, and $[I_{\text{sc},B}]$ is the inertia tensor of the spacecraft about point B. Additionally, N_{eff} is the number of effectors to be summed over, $\boldsymbol{F}_{\text{ext}}$ is the total external force applied to the spacecraft, and $\boldsymbol{L}_B$ is the total external torque applied to the spacecraft. $\boldsymbol{v}_{\text{Trans,RHS}_i}$ and $\boldsymbol{v}_{\text{Rot,RHS}_i}$ are the vector contribution to the forces and torques respectively of effector i, and $\boldsymbol{v}_{\text{Trans,LHS}_i}$ and $\boldsymbol{v}_{\text{Rot,LHS}_i}$ are the vectors for the translational and rotational equations respectively that correspond with effector i's second order derivative of its state. Finally, $\boldsymbol{a}_{\alpha_i}$, $\boldsymbol{b}_{\alpha_i}$, and c_{α_i} are

the coefficients from the EOM of effector i relating its second order state $\ddot{\alpha}_i$ to the second order hub translational and rotational states as shown in Eq. (4).

$$\ddot{\alpha}_i = \boldsymbol{a}_{\alpha_i} \cdot \ddot{\boldsymbol{r}}_{B/N} + \boldsymbol{b}_{\alpha_i} \cdot \dot{\boldsymbol{\omega}}_{\mathcal{B}/\mathcal{N}} + c_{\alpha_i} \tag{4}$$

The numerical speed of the BSM method is achieved because the numerical inversion of the typical large system mass matrix is avoided by analytically solving for the $\boldsymbol{v}_{\text{Trans}}$ and $\boldsymbol{v}_{\text{Rot}}$ terms for each effector. Prior work has developed BSM solutions for a range of state effector such as single- and dual-hinged panels, generally spinning bodies, balanced and imbalanced reaction wheels.[23,26,30] However, this prior work assumes a series of state and dynamic effectors are attached to the central hub, but does not allow dynamic effectors to be attached to state effector components which would yield some branch capability in the dynamic modeling of a complex spacecraft system.

ADD SELECT BRANCHING TO STATE EFFECTOR

Now, knowing the required form of the EOMs of the spacecraft hub and its components for an architecture in which all components are mounted directly to the hub, specific terms can be altered to instead enable linking a dynamic effector to a state effector. First focusing on the dynamic effector which contributes external forces and torques to the spacecraft without any states α_i of its own to be integrated. These forces and torques are previously summed up as $\boldsymbol{F}_{\text{ext}}$ and $\boldsymbol{L}_B$ in Eqs. (3a) and (3b) for the hub motion assuming that those forces and torques are transferred to the hub without loss. Instead, external forces and torques must now be taken into account in the EOM of the intermediate platform first.

With Basilisk's spinning bodies chosen as the intermediate platform, its back-substitution formulated EOM from reference (31) for a single rotating segment is shown in Eqs. (5)-(10) with the additional term from all attached components highlighted in blue. Without loss of generality this derivation of a single rotating segment can also be performed for multiple segments.

$$\ddot{\theta} = \boldsymbol{a}_\theta \cdot \ddot{\boldsymbol{r}}_{B/N} + \boldsymbol{b}_\theta \cdot \dot{\boldsymbol{\omega}}_{\mathcal{B}/\mathcal{N}} + c_\theta \tag{5}$$

$$\boldsymbol{a}_\theta = \frac{m_{\text{S}}}{m_\theta}[\tilde{\boldsymbol{r}}_{S_c/S}]\hat{\boldsymbol{s}} \tag{6}$$

$$\boldsymbol{b}_\theta = -\frac{1}{m_\theta}\left([I_{\text{S},S}] - m_{\text{S}}[\tilde{\boldsymbol{r}}_{S/B}][\tilde{\boldsymbol{r}}_{S_c/S}]\right)\hat{\boldsymbol{s}} \tag{7}$$

$$c_\theta = \frac{1}{m_\theta}(u_{\text{S}} - \hat{\boldsymbol{s}}^T(\boldsymbol{L}_{\text{S}} + [\tilde{\boldsymbol{\omega}}_{\mathcal{S}/\mathcal{N}}][I_{\text{S},S}]\boldsymbol{\omega}_{\mathcal{S}/\mathcal{N}} + [I_{\text{S},S}][\tilde{\boldsymbol{\omega}}_{\mathcal{B}/\mathcal{N}}]\boldsymbol{\omega}_{\mathcal{S}/\mathcal{B}} + m_{\text{S}}[\tilde{\boldsymbol{r}}_{S_c/S}][\tilde{\boldsymbol{\omega}}_{\mathcal{B}/\mathcal{N}}]\dot{\boldsymbol{r}}_{S/B})) \tag{8}$$

$$\boldsymbol{F}_{\text{S}} = \sum_{i=1}^{N_{eff}} \boldsymbol{F}_{\text{i}} \qquad \boldsymbol{L}_{\text{S}} = \sum_{i=1}^{N_{eff}} \boldsymbol{L}_{\text{i}} \tag{9}$$

$$m_\theta = \hat{\boldsymbol{s}}^T[I_{\text{S},S}]\hat{\boldsymbol{s}} \tag{10}$$

The platform's state is its angle orientation θ about axis $\hat{\boldsymbol{s}}$ in the platform's local body fixed frame $\mathcal{S}$ at point S. The mass of the spinning body is m_{S} with its COM at point S_c and the mass-like term m_θ is divided through to isolate the state variable. There is a control torque u_{S} for actuated control

of the spinning body's orientation, and now an additional torque $\boldsymbol{L}_{\text{S}}$ representing the total torque from attached components about local frame origin S. The component of the torque parallel to the spin axis is isolated here through its dot product with the spin axis $\hat{\boldsymbol{s}}$. The total external torque on the vehicle must also be accumulated through $\boldsymbol{v}_{\text{Rot,RHS}}$ in the equation updated from reference (31) shown in Eq. (11). Added terms are again highlighted in blue.

$$\begin{aligned}\boldsymbol{v}_{\text{Rot,RHS}} = &-[\tilde{\boldsymbol{\omega}}_{\mathcal{S}/\mathcal{N}}][I_{\text{S},S_c}]\boldsymbol{\omega}_{\mathcal{S}/\mathcal{B}} - m_{\text{S}}[\tilde{\boldsymbol{\omega}}_{\mathcal{B}/\mathcal{N}}][\tilde{\boldsymbol{r}}_{S_c/B}]\boldsymbol{r}'_{S_c/B} \\ &- m_{\text{S}}[\tilde{\boldsymbol{r}}_{S_c/B}][\tilde{\boldsymbol{\omega}}_{\mathcal{S}/\mathcal{B}}]\boldsymbol{r}'_{S_c/S} + \boldsymbol{L}_{\text{S}} + [\tilde{\boldsymbol{r}}_{S/B}]\boldsymbol{F}_{\text{S}} \end{aligned} \tag{11}$$

Also present in Eq. (11) is an additional torque computed from the total force contributed by attached components $\boldsymbol{F}_{\text{S}}$. This force does not appear in the individual EOM for the spinning body state θ as the torque output from dynamic effectors already accounts for torques imparted by the forces it generates. However, this torque $\boldsymbol{L}_{\text{S}}$ as suggested by its subscript is computed about local frame origin S, and the torque contributed to $\boldsymbol{v}_{\text{Rot,RHS}}$ is applied about body frame origin B. This total force imparted by attached components F_{S} is also factored into the updated equation for $\boldsymbol{v}_{\text{Trans,RHS}}$ as highlighted in blue in Eq. (12).

$$\boldsymbol{v}_{\text{Trans,RHS}} = -m_{\text{S}}[\tilde{\boldsymbol{\omega}}_{\mathcal{S}/\mathcal{B}}]\boldsymbol{r}'_{S_c/S} + \boldsymbol{F}_{\text{S}} \tag{12}$$

This mathematical formulation has been derived in a frame-agnostic way, but in implementation in Basilisk will have frames assigned for each specific vector. It is important that frames are held consistent throughout the equation, and in the existing Basilisk framework the local body frame $\mathcal{B}$ is chosen when computing backsubstitution parameters. Because of this, the forces and torques output by dynamic effectors are produced in its local parent frame, which has traditionally been the body frame. However, with this new branching of the dynamic effectors off of state effectors, the local parent frame is not the body frame, and the state effector must rotate these collected forces and torques to the body frame when computing back-substitution parameters.

NUMERICAL RESULTS

How the dynamics of a space vehicle are modeled is largely dependent on the solver used, and therefore the simulation framework in which they are implemented. When considering time-varying geometries for a multibody dynamical system, the equations of motion are a coupled nonlinear set which may be organized in different forms depending on the solving technique to be used. Although there are a multitude of software packages that utilize different techniques, this project seeks a simulation framework that is 1) computationally efficient at solving the coupled nonlinear equations, 2) tailored to spacecraft components and environments, and 3) open source such that the underlying dynamics solver is available to be adapted. Based on these criteria, the Basilisk Simulation Framework* is chosen which leverages the back-substitution method (BSM) to modularize a spacecraft's equations of motion.[32] Basilisk has already been applied to the component categories of actuated and hub excited time-varying geometries.[16,26] While Basilisk's BSM is well tailored to the modular nature of spacecraft, it follows the common assumption first mentioned that spacecraft are organized as a set of components mounted to a central hub.[29] Therefore, the underlying technology required to model component excited flexing in a modular way is the ability to branch components.

There are three collections of state effectors in Basilisk which are able to model a moving platform: hinged rigid bodies, linear translation bodies, and spinning bodies. Linear translation bodies

*http://hanspeterschaub.info/basilisk

models linearly translating platforms. The hinged rigid bodies are a collection of successive platforms connected by hinges that all lie in the same direction, whereas the spinning bodies are a collection of successive platforms connected by hinges that can be oriented in any direction. Spinning bodies is chosen to be adapted in this work given its ability to model any set of spinning bodies, including those that hinged rigid bodies is capable of. This behavior best matches the robotic arms currently used in space, which rarely have linearly translating joints.

The dynamics of component excited flexing is first demonstrated in Basilisk by a thruster dynamic effector mounted to a 1-DOF spinning body state effector replicating a gimbaled thruster. The input parameters corresponding to these components are shown in Table 1, and the spacecraft as well as the spinning body platform start at rest. At ten seconds into the simulation the thruster is turned on at full thrust for thirty seconds and then shut off at forty seconds in.

Table 1. Simulation parameters for gimballed thruster.

Parameter	Notation	Value	Units
Spacecraft mass	m_{sc}	400	kg
Spacecraft inertia about its COM	${}^{\mathcal{B}}[I_{\text{sc},B}]$	$\begin{bmatrix} 633 & 0 & 0 \\ 0 & 633 & 0 \\ 0 & 0 & 200 \end{bmatrix}$	kg·m^2
Spinning body mass	m_S	50	kg
Spinning body inertia about its COM	${}^{\mathcal{S}}[I_{\text{S},S_c}]$	$\begin{bmatrix} 50 & 0 & 0 \\ 0 & 30 & 0 \\ 0 & 0 & 40 \end{bmatrix}$	kg·m^2
Spinning body frame origin location in the body frame	${}^{\mathcal{B}}\boldsymbol{r}_{S/B}$	${}^{\mathcal{B}}[1,0,0]^T$	m
Spinning body COM in its local frame	${}^{\mathcal{S}}\boldsymbol{r}_{S_c/S}$	${}^{\mathcal{B}}[0.5,0,0]^T$	m
Spinning body spin axis in its local frame	${}^{\mathcal{S}}\hat{\boldsymbol{s}}$	${}^{\mathcal{S}}[0,1,0]^T$	m
DCM of the $\mathcal{S}$ frame with respect to the $\mathcal{B}$ frame	$[\mathcal{SB}]$	$\begin{bmatrix} 1 & 0 & 0 \\ 0 & 1 & 0 \\ 0 & 0 & 1 \end{bmatrix}$	–
Spinning body joint stiffness	k	100	N·m/rad
Spinning body joint damping	c	50	N·m·s/rad
Thruster position in spinning body frame	${}^{\mathcal{S}}\boldsymbol{r}_{T/S}$	${}^{\mathcal{S}}[1,0,0]^T$	m
Thrust direction in spinning body frame	${}^{\mathcal{S}}\hat{\boldsymbol{t}}$	${}^{\mathcal{S}}[0,0,-1]^T$	-
Thruster max thrust	F_{Tmax}	4.5	N

Two spacecraft are simulated with these same parameters. One with the new component excited flexing such that the thruster is mounted directly to the flexible platform, and the other using the default methodology in which the thruster is positioned at the same starting location, but applies its forces and torques to the central hub. The resulting motion of the flexible moving platform is shown for both spacecraft in Figure 4.

To study changes in the resulting motion of the spacecraft, Figures 5 through 8 show the central hub translational position and velocity as well as attitude and angular rate for the same thruster firing.

With the 1-DOF serving as a proof-of-concept for the branching, the method can now be stress tested against more complex scenarios. Firstly, adding degrees of freedom to the motion platform, in this case a series of revolute spinning bodies, can be performed. Extending to 2-DOF but keeping

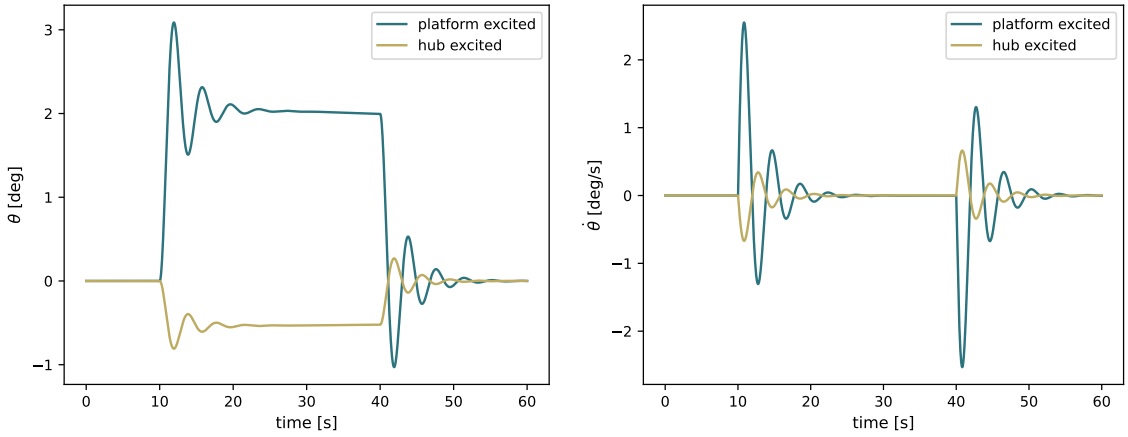

(a) Orientation angle

(b) Orientation angle rate of change

Figure 4. 1-DOF spinning body platform motion with thruster firing.

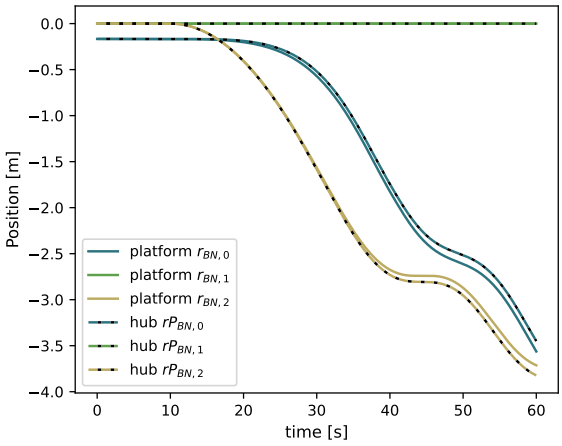

Figure 5. Hub position with thruster firing.

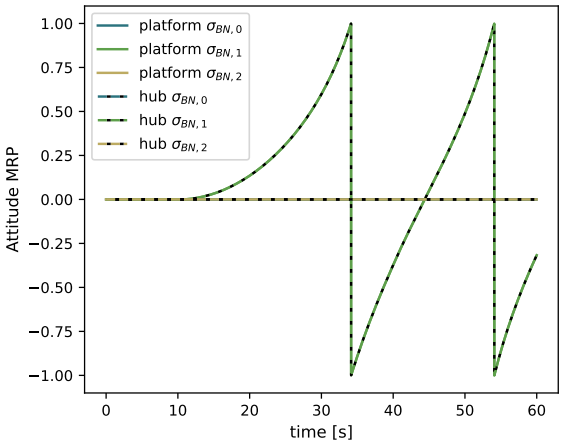

Figure 6. Hub attitude with thruster firing.

a thruster attached to the farthest segment from the central hub produces the angular motion at each joint shown in Figure 9.

DISCUSSION

The primary benefit of modeling component excited flexing is immediately apparent in Figure 4, in that the resulting deflection of the intermediate platform occurs in opposite directions. When forces and torques are sent directly to the central hub, the moving platform lags behind in motion, whereas the actual phenomenon is the opposite: the forces and torques are being applied at the moving platform and it is the central hub that lags behind in motion. Furthermore, the same magnitude of thrust results when applied to the mass of a platform in contrast to the mass of the central hub incites a larger acceleration, and therefore a larger deflection of the panel.

Then, studying the resulting motion of the central hub, slight differences in each state are noted. The angular velocity shown in Figure 8 varies during the transients at thruster on and off at ten

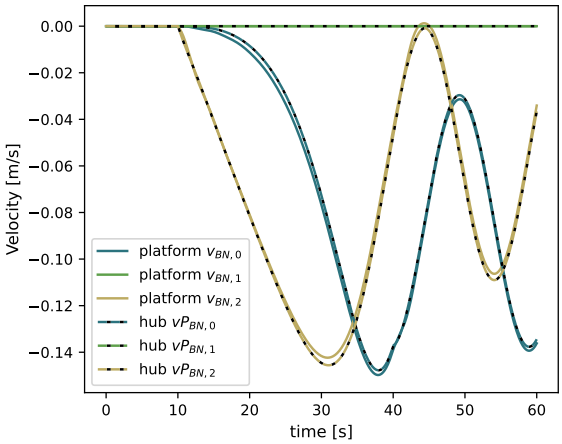

Figure 7. Hub velocity with thruster firing.

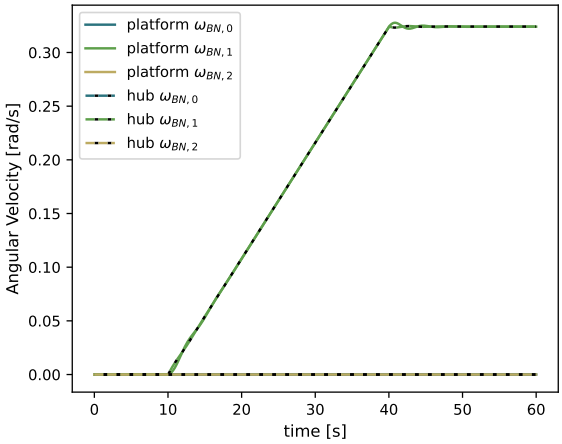

Figure 8. Hub angular velocity with thruster firing.

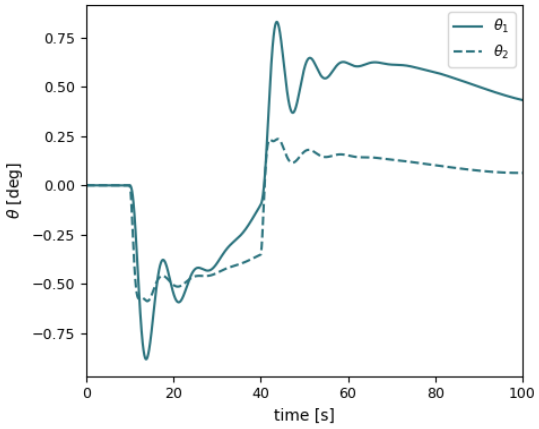

(a) Orientation angles

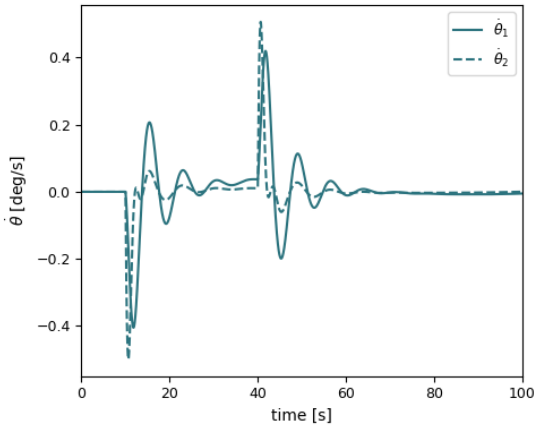

(b) Orientation angle rates of change

Figure 9. 2-DOF spinning body platform motion with thruster firing.

and forty seconds, respectively, into the simulation. The associated attitude varies more subtly with angular velocity variations isolated to the transients. The linear velocity shows a more appreciable variation past the transient due to the compounded change in force application direction as the attitude drifts, and that drift is further compounded at the translational position differences shown in Figure 5.

Looking to the stress test cases, the dynamical coupling is enabled for motion platforms of multi-DOF. Figure 9(a) shows slower settling times compared to the 1-DOF case, since the thruster is mounted at a greater distance from the vehicle's center of mass and thus results in a larger spin. Because of this, the arm begins to lag behind the hub's spin after the thruster finishes firing, and initial settling oscillations damp out.

CONCLUSION

This alteration to the BSM surmounts a limitation of Basilisk which previously could not perform branching of components while maintaining its modular architecture. The selective configuration space of branching enables dynamic effectors capable of generating forces and torques to be attached to the spinning bodies state effector capable of modeling rotationally time-varying geometries.

While single DOF spinning bodies was adapted to accommodate attached dynamic effectors in this work, an N-DOF spinning bodies state effector now exists which enables a generalized set of spinning bodies of any number of successive platforms. Future work at the back-substitution level aims to adapt the attachment of dynamic effectors to this N-DOF model, enabling an even larger configuration space of branching.

This branching also enables further complexity at the scenario level. Future work of interest includes modeling a moving platform as a more significant portion of the spacecraft such as a dual spinner, which may have multiple components attached to the intermediate platform. Additionally, scenarios can be expanded at the controls level to study differences in the resulting motion and resonance analysis with pulsed thrust control.

ACKNOWLEDGMENT

This work is supported by a NASA Space Technology Graduate Research Opportunity (NSTGRO) grant, 80NSSC24K1394.

REFERENCES

[1] C. Allard, M. Diaz-Ramos, P. W. Kenneally, H. Schaub, and S. Piggott, "Modular Software Architecture for Fully-Coupled Spacecraft Simulations," *Journal of Aerospace Information Systems*, Vol. 15, No. 12, 2018, pp. 670–683, 10.2514/1.I010653.

[2] C. Allard, M. Diaz-Ramos, and H. Schaub, "Computational Performance of Complex Spacecraft Simulations Using Back-Substitution," *Journal Of Aerospace Information Systems*, Vol. 16, Oct. 2019, pp. 427–436, 10.2514/1.I010713.

[3] SpaceLogistics, "Mission Extension Vehicle (MEV) Fact Sheet," 2021.

[4] T. Harris, H. Brettle, M. Lecas, L. Blacketer, A. Carr, A. Fernandez, and A. Puppa, "An exploration of opportunities to advance ground-based and space-based SSA systems through in-orbit demonstration missions," *8th European Conference on Space Debris*, April 2021.

[5] NASA/JPL-Caltech, "Mars Reconnaissance Orbiter, Aerobraking," `https://science.nasa.gov/resource/mars-reconnaissance-orbiter-aerobraking/`, July 14 2009.

[6] R. W. Shane and R. H. Tolson, *Aerothermodynamics of the Mars Global Surveyor Spacecraft*. Hampton, VA: NASA, Langley Research Center, 1998.

[7] R. Biesbroek, S. Aziz, A. Wolahan, S.-f. Cipolla, M. Richard-Noca, and L. Piguet, "The clearspace-1 mission: Esa and clearspace team up to remove debris," *Proc. 8th Eur. Conf. Sp. Debris*, 2021, pp. 1–3.

[8] S. Space, "Otter is there, on call and ready to support.," `https://www.starfishspace.com/the-otter/`, 2023.

[9] M. A. Shoemaker, M. Vavrina, D. E. Gaylor, R. Mcintosh, M. Volle, and J. Jacobsohn, "OSAM-1 decommissioning orbit design," *AAS/AIAA Astrodynamics Specialis t Conference*, 2020.

[10] R. Staples, "Key Capabilities of our Life Extension In-orbit (LEXI™) Servicer," `https://astroscale-us.com/lexi-life-extension-capabilities/`, October 2021.

[11] A. Eisele, "Northrop Grumman's SpaceLogistics Continues Revolutionary Satellite Life-Extension Work with Sale of Third Mission Extension Pod," `https://news.northropgrumman.com/news/releases/northrop-grummans-spacelogistics-continues-revolutionary-satellite-life-extension-work-with-sale-of-third-mission-extension-pod`, June 2023.

[12] A. K. Banerjee, "Contributions of Multibody Dynamics to Space Flight: A Brief Review," *Journal of Guidance, Control, and Dynamics*, Vol. 26, No. 3, 2003, pp. 385–394, 10.2514/2.5069.

[13] A. Jain, "Unified formulation of dynamics for serial rigid multibody systems," *Journal of Guidance, Control, and Dynamics*, Vol. 14, No. 3, 1991, pp. 531–542, 10.2514/3.20672.

[14] T. R. Kane and D. A. Levinson, "Formulation of equations of motion for complex spacecraft," *Journal of Guidance and control*, Vol. 3, No. 2, 1980, pp. 99–112.

[15] A. Jain and G. Rodriguez, "Recursive dynamics algorithm for multibody systems with prescribed motion," *Journal of guidance, control, and dynamics*, Vol. 16, No. 5, 1993, pp. 830–837.

[16] L. Kiner, J. Vaz Carneiro, A. Cody, and H. Schaub, "Spacecraft Simulation Software Implementation Of General Prescribed Motion Dynamics Of Two Connected Rigid Bodies," *AAS Guidance and Control Conference*, Breckenridge, CO, Feb. 2–8 2023. Paper No. AAS-23-084.

[17] L. Kiner, C. Allard, and H. Schaub, "Multi-Body Prescribed Spacecraft Dynamics Subject To Actuator Inputs," *AAS/AIAA Astrodynamics Specialist Conference*, Big Sky, MO, Aug. 13–17 2023. Paper AAS 23–230.

[18] L. Kiner, C. Allard, and H. Schaub, "Prescribed Motion Dynamics For Spacecraft Solar Array Deployment," *AAS Guidance and Control Conference*, Breckenridge, CO, Feb. 2–7 2024. Paper No. AAS 24-123.

[19] C. Allard, H. Schaub, and S. Piggott, "General Hinged Solar Panel Dynamics Approximating First-Order Spacecraft Flexing," *AIAA Journal of Spacecraft and Rockets*, Vol. 55, No. 5, 2018, pp. 1290–1298, 10.2514/1.A34125.

[20] A. Grewal and V. J. Modi, "Multibody dynamics and robust control of flexible spacecraft," *IEEE Transactions on Aerospace and Electronic Systems*, Vol. 36, No. 2, 2000, pp. 491–500.

[21] C. Allard, M. Diaz-Ramos, and H. Schaub, "Spacecraft Dynamics Integrating Hinged Solar Panels and Lumped-Mass Fuel Slosh Model," *AIAA/AAS Astrodynamics Specialist Conference*, Long Beach, CA, Sept. 12–15 2016.

[22] P. Cappuccio, C. Allard, and H. Schaub, "Fully-Coupled Spherical Modular Pendulum Model To Simulate Spacecraft Propellant Slosh," *AAS/AIAA Astrodynamics Specialist Conference*, Snowbird, UT, August 19–23 2018. Paper No. AAS-18-224.

[23] J. Vaz Carneiro, C. Allard, and H. Schaub, "General Dynamics for Single- and Dual-Axis Rotating Rigid Spacecraft Components," *Journal of Spacecraft and Rockets*, Vol. 61, July–August 2024, pp. 1099–1113, 10.2514/1.A35865.

[24] J. Vaz Carneiro, P. Johnson, and H. Schaub, "Backsubstitution Method For Spacecraft With Generally Translating Appendages," *AAS Astrodynamics Specialist Conference*, Broomfield, CO, Aug. 11–15 2024. Paper No. AAS 24-248.

[25] B. Wie, N. Furumoto, A. Banerjee, and P. Barba, "Modeling and simulation of spacecraft solar array deployment," *Journal of Guidance, Control, and Dynamics*, Vol. 9, No. 5, 1986, pp. 593–598.

[26] G. Bascom and H. Schaub, "Modular Dynamic Modeling Of Hinged Solar Panel Deployments," *AAS Astrodynamics Specialist Conference*, Charlotte, NC, Aug. 7–10 2022. Paper No. AAS 22-725.

[27] J. Vaz Carneiro and H. Schaub, "Spacecraft Dynamics With The Backsubstitution Method: Survey And Capabilities," *AAS Spaceflight Mechanics Meeting*, Kauai, Hawaii, Jan. 19–23 2025. Paper No. AAS 25-232.

[28] A. Morell and H. Schaub, "Back-Substitution Based Spacecraft Dynamics Modeling With Selective Configuration Space Branching," *AAS Astrodynamics Specialist Conference*, Broomfield, CO, Aug. 11–15 2024. Paper No. AAS 24-361.

[29] C. Allard, M. Diaz-Ramos, P. W. Kenneally, H. Schaub, and S. Piggott, "Modular Software Architecture for Fully-Coupled Spacecraft Simulations," *Journal of Aerospace Information Systems*, Vol. 15, No. 12, 2018, pp. 670–683, 10.2514/1.I010653.

[30] J. Alcorn, C. Allard, and H. Schaub, "Fully Coupled Reaction Wheel Static and Dynamic Imbalance for Spacecraft Jitter Modeling," *AIAA Journal of Guidance, Control, and Dynamics*, Vol. 41, No. 6, 2018, pp. 1380–1388, 10.2514/1.G003277.

[31] J. Vaz Carneiro, C. Allard, and H. Schaub, "Rotating Rigid Body Dynamics Architecture For Spacecraft Simulation Software Implementation," *AAS Guidance and Control Conference*, Breckenridge, CO, Feb. 2–8 2023. Paper No. AAS-23-112.

[32] P. W. Kenneally, S. Piggott, and H. Schaub, "Basilisk: A Flexible, Scalable and Modular Astrodynamics Simulation Framework," *Journal of Aerospace Information Systems*, Vol. 17, Sept. 2020, pp. 496–507.